COLLISION AND TURNOVER AVOIDANCE OF MOBILE ROBOTS WITH FORCE REFLECTION

Jae Byung Park*, Jeong Hee Lee*, Gon Woo Kim* and Beom Hee Lee**

**Ph.D. Student and **Professor, School of Electrical Engineering*
Seoul National University, Seoul, Korea
E-mail: pjb0922@snu.ac.kr

Abstract: Collision and turnover are fatal to mobile robots. Control methods are suggested for solving the fatal problems of mobile robots maneuvered by an operator. Speed reduction and wall following are applied for collision avoidance using ultrasonic sensor data. Modified Hough transform is suggested to obtain a wall model from sonar data overcoming limitations of ultrasonic sensors. The robot is also controlled by constraints of turnover using front terrain data. To predict the data about front terrain, a low-cost terrain sensor module is developed. Besides, to recognize the robot movement controlled for guaranteeing safety, a force reflection technique is applied. *Copyright © 2005 IFAC*

Keywords: obstacle avoidance, turnover avoidance, force reflection, mobile robots

1. INTRODUCTION

In mobile robot applications, collision and turnover are very important problems to be solved. The robot used in this paper, ROBHAZ-DT, is developed by the Korea Institute of Science and Technology (KIST) for operating in minefield. In the case of the ROBHAZ-DT, one of mobile robots which operate in hazardous environment such as nuclear power plant and minefield, collision and turnover of the robot body during operation is fatal. Therefore, this paper focuses on collision and turnover avoidance for mobile robots.

A whole system consists of a Remote Monitoring System (RMS) and a Mobile Robot System (MRS) as shown in Fig. 1. The RMS and the MRS communicate with each other via wireless Ethernet.

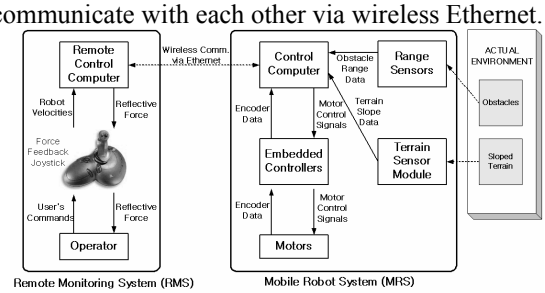

Fig. 1. Whole System consisting of the RMS and the MRS

The RMS interfaces with a force feedback joystick which is a kind of 2 DOF (Degree Of Freedom) haptic devices based on Virtual Reality (Bauzil, 1981). Therefore, the RMS can receive the operator's command and feed back reflective force into the operator. The user's commands consist of the forward and the angular velocities determined by the joystick positions about the Y-axis and the X-axis, respectively. Here, the controlled robot movement for collision and turnover avoidance is monitored by the reflective force. The algorithms for collision and turnover avoidance are included in the RMS. Next, the MRS controls the actual motors and receives encoder, ultrasonic sensor and terrain sensor data. A semicircular ultrasonic sensor array is used for obstacle avoidance (Borenstein, 1989) considering the limitations of the sensors (Borenstein, 1995). Also, a low-cost terrain sensor module, consisting of a laser line generator, a web camera and an inclinometer, is developed for turnover avoidance.

This paper is organized as follows. In Section 2, the mobile robot control methods for collision and turnover avoidance are suggested. Also, the reflective force for recognizing the actual movement of the robot is described. In Section 3, experimental results of the suggested methods are described. Finally, conclusions are presented in Section 4.

2. MOBILE ROBOT CONTROL

2.1 Obstacle Avoidance Control

The forward and the angular velocities of the robot are controlled for obstacle avoidance using a semicircular sonar array consisting of 8 sonar sensors. First, the forward velocity is controlled by obstacle sparseness (Fukuda, 1995). The update equation of sparseness $sprs(k)$ of obstacles at discrete time k is defined as

$$sprs(k+1)=\begin{cases}\gamma^{-1}\cdot sprs(k), & if\ {}^{\forall}D_{\mathrm{n}}\geq A\_rng(k)\\ \gamma\cdot sprs(k), & otherwise\end{cases} \quad (1)$$

where γ is a perception coefficient with the range $0<\gamma<1$, D_{n} is a distance between the robot center and the obstacle detected by the $\mathrm{n_{th}}$ sonar sensor where n=1,2,…,8, and $A\_rng(k)$ is an attention range of the sonar sensors. The sparseness is defined within $0<sprs_{\min}\leq sprs(k)\leq 1$ where $sprs_{\min}$ is the minimum value of the sparseness. Also, the attention range is recursively defined by the sparseness as

$$A\_rng(k)=sprs(k)\cdot D_{\max} \quad (2)$$

where $D_{\max}$ is a maximum range of sonar sensors. By the sparseness, an upper limit of the forward velocity for avoiding potential collision with obstacles is defined as

$$v_{\mathrm{sprs}}(k)=sprs(k)\cdot v_{\max} \quad (3)$$

where $v_{\max}$ is a maximum forward velocity of the robot. Therefore, the resultant forward velocity is defined by the command $v_{\mathrm{cmd}}(k)$ of an operator and $v_{\mathrm{sprs}}(k)$ as

$$v(k)=\min\left(v_{\mathrm{cmd}}(k),v_{\mathrm{sprs}}(k)\right)\cdot\left(1-e^{-\eta\cdot\left(\max\left(\min(D_1,\Lambda,D_8),D_{\min}\right)-D_{\min}\right)}\right) \quad (4)$$

where $D_{\min}$ is a minimum permissible distance between the robot and obstacles, and η is a decreasing ratio. By (4), the command $v_{\mathrm{cmd}}(k)$ is limited by $v_{\mathrm{sprs}}(k)$ for avoiding potential collision. The resultant forward velocity is also exponentially reduced to prevent the robot from approaching obstacles and is eventually determined as zero when the distance from obstacles is closer than $D_{\min}$.

Next, the angular velocity of the robot is controlled for wall following. The parameters of a wall model consist of a distance ρ' between the robot center position (RCP) and the wall and an angle θ' between the normal vector of the wall and the X_r-axis of the robot frame {R} as shown in Fig. 2 (a). To obtain the wall model parameters from sonar data, a modified Hough transform is suggested, and the transform has 4 steps as follows:

[Step1] Quantize the θ-ρ parameter space appropriately.

[Step2] Assume that each cell in the parameter space is an accumulator. Initialize all cells to zero.

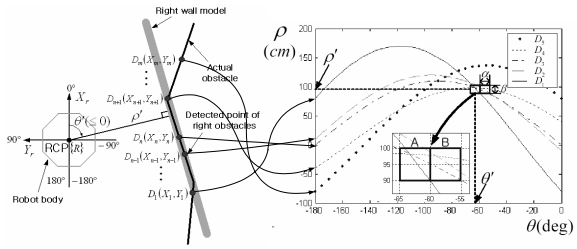

Fig. 2. Modified Hough Transform : (a) wall model parameters with 5 detected points (b) θ-ρ parameter space

[Step3] For each point $(X_{\mathrm{n}}, Y_{\mathrm{n}})$ measured by the $\mathrm{n_{th}}$ sonar sensor, increment by ζ_{n} each of the accumulators that satisfy the equation $\rho=X_{\mathrm{n}}\cos\theta+Y_{\mathrm{n}}\sin\theta$ where n=1,2,…,8.

[Step4] Maximum in the accumulator array correspond to the parameters of a model instance.

In [step3], the increasing step is not 1 but ζ_{n}. It is the main difference from the original Hough transform. The increasing step ζ_{n} is defined as

$$\zeta_{\mathrm{n}}=\begin{cases}2, & \theta_{\mathrm{n}}=\theta_{\mathrm{ref}}\\ 1, & \left|\theta_{\mathrm{ref}}-\theta_{\mathrm{n}}\right|\leq\theta_{\mathrm{sr}}\left(\theta_{\mathrm{n}}\neq\theta_{\mathrm{ref}}\right)\\ 0, & otherwise\end{cases} \quad (5)$$

where θ_{ref} is the angle between the X_r-axis and the acoustic axis of the sonar sensor which measures the minimum distance among the 8 sensors, and θ_{sr} is the angle for specular reflection of sonar sensors. An example of the modified Hough transform is shown in Fig. 2. There are 5 detected points relative to {R} such as D_1(-80, -150), D_2(-10, -120), D_3(0, -110), D_4(40, -90) and D_5(80, -100) where the points are assumed to satisfy the condition $\left|\theta_{\mathrm{ref}}-\theta_{\mathrm{n}}\right|\leq\theta_{\mathrm{sr}}$ of (5) for n=1,2,…,5. In this example, θ_4 is set as θ_{ref} since D_4 is the minimum distance among the 5 points. Therefore, the increasing steps for the points are determined as ζ_1=1, ζ_2=1, ζ_3=1, ζ_4=2 and ζ_5=1. Then, each of the accumulators in the θ-ρ parameter space which satisfy the equation $\rho=X_{\mathrm{n}}\cos\theta+Y_{\mathrm{n}}\sin\theta$ is incremented by ζ_{n} for n=1,2,…,5 as shown in Fig. 2 (b). In result, the cell A is the maximum in the parameter space where ρ'=95 *cm* and θ'=-62.5º where θ' and ρ' are quantized by α=5º and β=10 *cm*, respectively. Next, by ρ' and θ', control parameters for wall following are defined as

$$D_{\mathrm{diff}}=sign(\theta')\cdot(\rho'-D_{\mathrm{ref}}) \quad (6)$$

$$\theta_{\mathrm{wall}}=-sign(\theta')\cdot(90^{\circ}-\left|\theta'\right|) \quad (7)$$

where D_{diff} is a distance between the distance ρ' and the reference distance D_{ref} for wall following, and an angle θ_{wall} between the heading direction of the robot and the wall. Using the control parameters, the angular velocity is determined for wall following as

$$\omega_{\mathrm{d}}(k)=(\xi_1(D_{\mathrm{diff}})+\xi_2(D_{\mathrm{diff}},\theta_{\mathrm{wall}}))\cdot\omega_{\max} \quad (8)$$

where

$$\xi_1(D_{\mathrm{diff}})=\frac{D_{\mathrm{diff}}}{D_{\mathrm{ref}}} \quad (9)$$

$$\xi_2(D_{\text{diff}},\theta_{\text{wall}})=\left(1-\left|\frac{D_{\text{diff}}}{D_{\text{ref}}}\right|\right)\cdot\left(\frac{\theta_{\text{wall}}}{2/3\cdot\theta_{\text{sr}}}\right) \tag{10}$$

In this case, the angular velocity $\omega_d(k)$ is applied to the robot when $v_{cmd}(k)>0.9\cdot v_{max}$ and $\rho' \le 2\cdot D_{ref}$, since the above conditions are regarded that the operator wants autonomous guidance for wall following.

2.2 Turnover Avoidance Control

The ROBHAZ-DT with a terrain sensor module is depicted in Fig. 3. In Fig. 4, a point $P_c(x_c, y_c, z_c)\in R^3$ on the laser line relative to the camera frame {C} can be obtained from a point $P_{img}(u, v)\in R^2$ on the camera image by comparing the similar triangles ΔP_cCM and $\Delta P_{img}M'C$ as

$$[x_c \quad y_c \quad z_c]=\frac{b}{f\cot\theta_{\text{lp}}+v}[f \quad u \quad v] \tag{11}$$

where b is a baseline distance between the center L of a laser line generator and the center C of a camera lens, f is a camera focal length, and θ_{lp} is a projection angle of a laser line into b. Next, in Fig. 5, the point P_c is transformed into the point $P_r(x_r, y_r, z_r)\in R^3$ relative to {R} as

$$\begin{bmatrix}x_r\\ y_r\\ z_r\\ 1\end{bmatrix}=\begin{bmatrix}\cos\theta_{rc} & 0 & \sin\theta_{rc} & 0\\ 0 & 1 & 0 & 0\\ -\sin\theta_{rc} & 0 & \cos\theta_{rc} & l_{rc}\\ 0 & 0 & 0 & 1\end{bmatrix}\begin{bmatrix}x_c\\ y_c\\ z_c\\ 1\end{bmatrix} \tag{12}$$

where the Y_r-axis is parallel with the Y_c-axis, l_{rc} is a distance between origins of {C} and {R}, and θ_{rc} is an angle between {R} and {C} about the Y_r-axis.

Then, in Fig. 6, a roll angle of the robot at $k+\Delta k_1$ is obtained relative to {R} as

$$\Delta\theta_{\text{Roll}}(k+\Delta k_1)=\tan^{-1}\left(\frac{z_{rL}(k)-z_{rR}(k)}{D_{\text{track}}}\right) \tag{13}$$

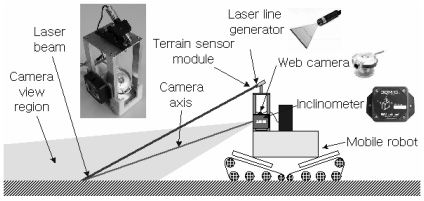

Fig. 3. ROBHAZ-DT with the Terrain Sensor

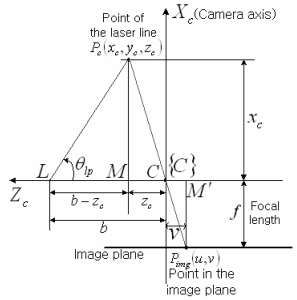

Fig. 4. Geometry Analysis of a Web Camera Image

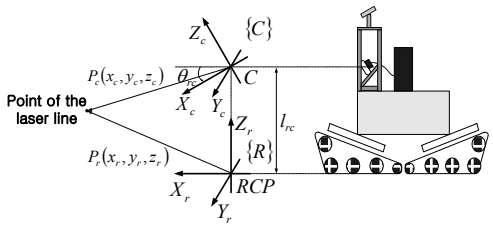

Fig. 5. Transform between Robot and Camera Frames, {R} and {C}

where D_{track} is a distance between two tracks of the robot. Here, $P_{rL}(k)$ and $P_{rR}(k)$, which are described as $(x_{rL}(k), y_{rL}(k), z_{rL}(k))$ and $(x_{rR}(k), y_{rR}(k), z_{rR}(k))$ respectively, are predicted positions of left and right tracks at $k+\Delta k_1$. The time Δk_1 is a minimum time satisfying

$$\begin{aligned}&\min\{x_{rL}(k), x_{rR}(k)\}\cdot\cos(\theta_{\text{3DM-Pitch}}(k))\\ &\le\sum_{n=0}^{\Delta k_1-1}v(k+n)\cdot T_s\cos(\theta_{\text{3DM-Pitch}}(k+n))\end{aligned} \tag{14}$$

where $\theta_{3DM\text{-}Pitch}(k)$ is a pitch angle of the robot at k relative to the universal frame, which is obtained by an inclinometer. Consequently, the predicted roll angle at $k+\Delta k_1$ is determined relative to the universal frame as

$$\hat{\theta}_{\text{Roll}}(k+\Delta k_1)=\theta_{\text{3DM-Roll}}(k)+\Delta\theta_{\text{Roll}}(k+\Delta k_1) \tag{15}$$

where $\theta_{3DM\text{-}Roll}(k)$ is a roll angle of the robot at k relative to the universal frame, which is also obtained by the inclinometer.

Next, in Fig. 7, a pitch angle of the robot at $k+\Delta k_1$ is obtained relative to {R} as

$$\Delta\theta_{\text{Pitch}}(k+\Delta k_1)=\tan^{-1}\left(\frac{z_{rF}(k)-z_{rF}(k-\Delta k_2)}{x_{rF}(k)-x_{rF}(k-\Delta k_2)}\right) \tag{16}$$

where Δk_2 is a minimum time satisfying the condition $L_{\text{fr}}\le\left|P_{rF}(k)P_{rF}(k-\Delta k_2)\right|$. Here, L_{fr} is a length between the front and the rear contact points of two tracks, and $\left|P_{rF}(k)P_{rF}(k-\Delta k_2)\right|$ is a distance between the point $P_{rF}(k)$ and the point $P_{rF}(k\text{-}\Delta k_2)$. The point $P_{rF}(k)$ of the front terrain at k is obtained by $P_{rL}(k)$ and $P_{rR}(k)$ as

$$\begin{aligned}P_{rF}(k)&=(x_{rF}(k), y_{rF}(k), z_{rF}(k))\\ &=\left(\min\{x_{rL}(k), x_{rR}(k)\}, \quad 0, \quad \frac{z_{rL}(k)+z_{rR}(k)}{2}\right)\end{aligned} \tag{17}$$

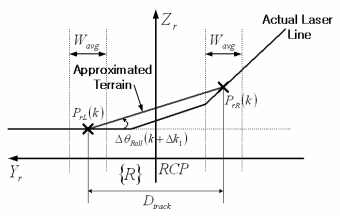

Fig. 6. Roll Angle Acquisition of the Front Terrain

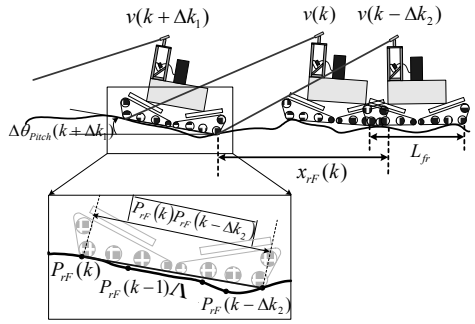

Fig. 7. Pitch Angle Acquisition of Front Terrain

In this case, for obtaining the distance $\left|P_{rF}(k)P_{rF}(k-\Delta k_2)\right|$, the point $P'_{rF}(k\text{-}\Delta k_2)$ relative to the robot frame defined at $k\text{-}\Delta k_2$ needs to be transformed into the point $P_{rF}(k\text{-}\Delta k_2)$ relative to the robot frame defined at k as

$$\begin{bmatrix} x_{rF}(k-\Delta k_2) \\ y_{rF}(k-\Delta k_2) \\ z_{rF}(k-\Delta k_2) \end{bmatrix} = \begin{bmatrix} x'_{rF}(k-\Delta k_2) \\ y'_{rF}(k-\Delta k_2) \\ z'_{rF}(k-\Delta k_2) \end{bmatrix} - \begin{bmatrix} \sum_{n=1}^{\Delta k_2} v(k-n)\cdot T_s \cdot \cos(\theta_{3DM-Pitch}(k-n)) \\ 0 \\ -\sum_{n=1}^{\Delta k_2} v(k-n)\cdot T_s \cdot \sin(\theta_{3DM-Pitch}(k-n)) \end{bmatrix} \quad (18)$$

where T_s is a communication period. Here, the second term of the right-hand side of (18) indicates a displacement vector between the robot frames at k and $k\text{-}\Delta k_2$. Consequently, the predicted pitch angle at $k+\Delta k_1$ relative to the universal frame is determined as

$$\hat{\theta}_{\text{Pitch}}(k+\Delta k_1) = \theta_{\text{3DM-Pitch}}(k) + \Delta\theta_{\text{Pitch}}(k+\Delta k_1) \quad (19)$$

Next, the motion equation of the robot suggested by Shiller (1991) is modified for a differential-drive robot with no predetermined path as

$$f_{X_r}\vec{X}_r + f_{Y_r}\vec{Y}_r + N\vec{Z}_r - mg\vec{Z}_u = mv\omega\vec{Y}_r + ma\vec{X}_r \quad (20)$$

where $\vec{X}_r$, $\vec{Y}_r$ and $\vec{Z}_r$ are unit vectors of each axis of {R}, and $\vec{Z}_u$ is an unit vector defined in the opposite direction of the gravity $[0\ 0\ -g]^T$. Here, f_{X_r}, f_{Y_r}, f_{Z_r} and N can be obtained by the projections of the external forces on the vectors $\vec{X}_r$, $\vec{Y}_r$ and $\vec{Z}_r$ as

$$f_{X_r} = mgk_{X_r} + ma \quad (21)$$

$$f_{Y_r} = mgk_{Y_r} + \frac{mv^2}{r} = mgk_{Y_r} + mv\omega \quad (22)$$

$$N = mgk_{Z_r} \quad (23)$$

where k_{X_r}, k_{Y_r} and k_{Z_r} are terrain parameters defined by the projections of the vector $\vec{Z}_u$ on the vectors $\vec{X}_r$, $\vec{Y}_r$ and $\vec{Z}_r$, respectively. Here, the terrain parameters can be obtained by the roll and the pitch angles such as $-\sin(\theta_{\text{Pitch}})$, $\sin(\theta_{\text{Roll}})\cos(\theta_{\text{Pitch}})$ and $\cos(\theta_{\text{Roll}})\cos(\theta_{\text{Pitch}})$, respectively. Next, the force distribution of the robot which is about to be overturned CCW and CW is depicted in Fig. 8 (a) and (b), respectively. Therefore, the turnover avoidance condition is defined as

$$-N\frac{W_r/2}{h} \le f_{Y_r} \le N\frac{W_r/2}{h} \quad (24)$$

where W_r is a width between two tracks, and h is a height of the center of mass of the robot. By substituting (22) and (23) into (24), (24) can be redefined about v and ω as

$$-g\left(k_{Y_r} + k_{Z_r}\frac{W_r/2}{h}\right) \le v\omega \le -g\left(k_{Y_r} - k_{Z_r}\frac{W_r/2}{h}\right) \quad (25)$$

where $v\omega$ is truncated by the range between $-v_{\max}\omega_{\max}$ and $v_{\max}\omega_{\max}$ considering the robot torque constraint. In result, the turnover-free range of the angular velocity at k is determined as

$$(v\omega)_{tr\_lb}/(v(k)+\Delta v) \le \omega(k) \le (v\omega)_{tr\_ub}/(v(k)+\Delta v) \quad (26)$$

where $(v\omega)_{\text{tr\_lb}}$ and $(v\omega)_{\text{tr\_ub}}$ are truncated bounds satisfying both (25) and the torque constraint. Here, Δv is defined as a maximum increase of the forward velocity: $\Delta v = -v(k) + \sqrt{v(k)^2 + 2aD_{\text{tp}}}$, when the robot moves the distance D_{tp}. Also, a is an acceleration of the robot, and D_{tp} is a reference distance from the front terrain for guaranteeing a minimum time to avoid turnover at k in advance. Therefore, the roll and the pitch angles of the robot at the front terrain already obtained at $k\text{-}\Delta k_3$ are applied for turnover avoidance at k, where Δk_3 is a minimum time satisfying

$$\min\{x_{rL}(k-\Delta k_3), x_{rR}(k-\Delta k_3)\}\cdot\cos(\theta_{\text{3DM-Pitch}}(k-\Delta k_3)) - \sum_{n=0}^{\Delta k_3-1} v(k-\Delta k_3+n)\cdot T_s\cos(\theta_{\text{3DM-Pitch}}(k-\Delta k_3+n)) \le D_{\text{tp}} \quad (27)$$

The resultant angular velocity determined by the command $\omega_{\text{cmd}}(k)$ of the operator or the reference velocity $\omega_{\text{d}}(k)$ for wall following is finally bounded by (26) for turnover avoidance.

2.3 Force Reflection

Reflective force of a force feedback joystick is fed back into the operator for recognizing the actual

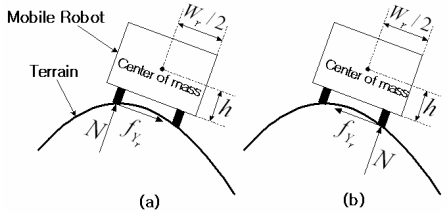

Fig. 8. Force Distribution of the Robot which is about to be overturned (a) CCW (b) CW

robot movement controlled for collision and turnover avoidance. In this paper, a position-based force heading for a reference point q_{offset} is used as shown in Fig. 9. Here, the force is not generated in the dead-band W_{DB}. Therefore, if the joystick position q is greater than $q_{\text{offset}}+W_{\text{DB}}$, the reflective force F_{P} with negative direction is generated, and vice versa. Here, joystick positions about the Y-axis and the X-axis range from -10000 to 10000 are scaled by the maximum forward and the maximum angular velocities of the robot, respectively.

For collision avoidance, the reference position q_{offset} about the Y-axis is determined by the upper limit of the forward velocity $v_{\text{sprs}}(k)$ and W_{DB} is set as 100. In this case, the magnitudes of F_{P} and F_{N} are set as 10000 and 0, respectively. Therefore, the operator feels the repulsive force preventing from his/her pushing the joystick forward whenever he/she pushes the joystick above the upper limit of the forward velocity. Also, the reference position q_{offset} about the X-axis is determined by the reference angular velocity $\omega_{\text{d}}(k)$ for wall following and W_{DB} is set as 100, when the wall following condition is satisfied. The magnitudes of F_{P} and F_{N} about the X-axis are set as 10000. In result, the operator can recognize that the robot is controlled for wall following. Next, in the case of turnover avoidance, q_{offset} and W_{DB} are determined as

$$\mathrm{q}_{\text{offset}} = 10000 \times \frac{1}{2}\left(\frac{(v\omega)_{tr\_lb} + (v\omega)_{tr\_ub}}{(v(k)+\Delta v)} \right) \Big/ \omega_{\max} \tag{28}$$

$$\mathrm{W}_{\text{DB}} = 10000 \times \frac{1}{2}\left(\frac{(vw)_{tr\_ub} - (vw)_{tr\_lb}}{(v(k)+\Delta v)} \right) \Big/ \omega_{\max} \tag{29}$$

By (28) and (29), the operator can recognize the upper and lower bounds of the angular velocity determined for turnover avoidance. Using the reflective force, the operator can always monitor the actual robot movement controlled for guaranteeing the safety.

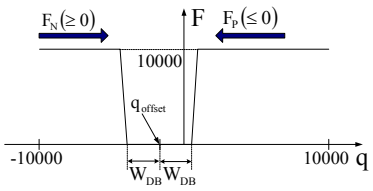

Fig. 9. Parameter Definition of the Position-Based Reflective Force

3. EXPERIMENTAL RESULTS

Experiments were carried out with the ROBHAZ-DT for verifying the validity of the suggested methods for collision and turnover avoidance. The sampling time T_{s} was set as 100 *ms* considering the sensor acquisition time. An experiment about collision avoidance was shown in Fig. 10. In this experiment, the robot moved for 30 seconds avoiding collision with two isolated obstacles and several wall-type

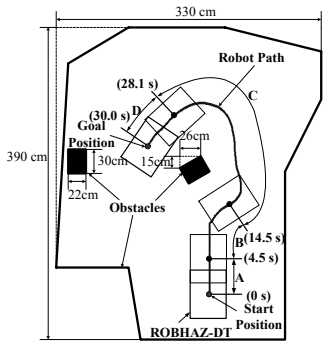

Fig. 10. Experimental Result of Collision Avoidance

obstacles. Here, the robot path was determined by the operator or the controller for collision avoidance. In this case, the maximum forward and the maximum angular velocities were set as 400 *mm/s* and 25 *deg/s*, respectively. According to the robot movement, the wall model parameters, the robot velocities, and the reflective force parameter were shown in Fig. 11. The wall model parameters in A, B and C sections were obtained by the modified Hough transform of left, front and right obstacles relative to the robot, respectively. In D section, the angle of the wall was repeatedly changed negative or positive, since the robot detected the left or right obstacle as the reference wall model. Here, the wall parameters, θ' and ρ', were quantized by α=5º and β=10 *cm*, respectively. Therefore, we could reduce the noise sensitivity of wall parameters. In E section, v_{sprs} was reduced from the initial value, and the forward velocity v was determined by v_{cmd} since v_{cmd} was less than v_{sprs}. In F section, v was reduced as zero by degrees for avoiding collision with the front obstacle which the robot continuously approached. In G section, the resultant angular velocity ω was controlled by ω_{d} for wall following since the wall-following conditions: $v_{\text{cmd}}(k)>0.9\cdot v_{\max}$ and $\rho' \le 2\cdot D_{\text{ref}}$, were satisfied. In this case, the operator felt the reflective force heading for the offset q_{offset} about the X-axis determined by ω_{d} where the dead-band W_{DB} of the reflective force was set as 100. In result, the operator could recognize that the robot was controlled for wall following. As the result of the

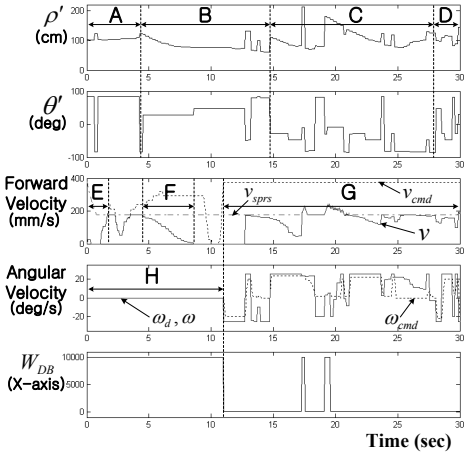

Fig. 11. Parameters about Experimental Result of Collision Avoidance

force, ω_{cmd} followed ω_d in Fig. 11. The reflective force about the X-axis, however, was not generated in H section since the wall-following condition, $v_{cmd}(k)>0.9 \cdot v_{max}$, was not satisfied. Therefore, the dead-band W_{DB} was set as 10000. For the forward velocity control, the reflective force about the Y-axis was generated whenever v_{cmd} was greater than v. In result, the operator could recognize the limited forward velocity for collision avoidance.

Next, experiments for turnover avoidance were carried out as shown in Fig. 12. The maximum forward and angular velocities were set as 860 *mm/s* and 90 *deg/s*, respectively. The reference distance D_{tp} was set as 50 *cm*. In the case of the robot path 1 in Fig. 12, the width W_r between two tracks and the height h of the center of mass of the robot were set as 48 *cm* and 25 *cm*, respectively. In this case, the turnover did not occur on the given sloped terrain. Therefore, the experiment for turnover avoidance was conducted after the height h was changed as 90 *cm*. In result, the robot moved along the robot path 2 for 6.3 seconds. The roll and pitch angles on the front terrain, the robot velocities, the joystick parameters and the reflective force parameter were depicted in Fig. 13. The roll and pitch angles at k indicated the angles predicted at k-Δk_3. In this case, the upper limit of the angular velocity ω_{tr_ub} was controlled for turnover avoidance as shown in Fig. 13. Therefore, the resultant angular velocity ω was determined by ω_{cmd} within the truncated range between ω_{tr_ub} and ω_{tr_lb}. Also, in Fig. 13, q_{offset} and W_{DB} of the reflective force about the X-axis were determined by ω_{tr_ub} and ω_{tr_lb}. The reflective force heading for the offset region defined by q_{offset} and W_{DB} was generated whenever the joystick position q was out of W_{DB}. Therefore, the operator could recognize the bounds of the angular velocity by the reflective force. In this experiment, the upper bound of the forward velocity was determined as the maximum velocity v_{max}. Therefore, the operator did not feel the reflective force about the Y-axis. As shown in the experimental results, the robot could move without collision and turnover and the operator could always recognize the actual robot movement by the reflective force.

4. CONCLUSION

The control methods for mobile robots maneuvered by an operator were suggested for avoiding collision and turnover. The speed reduction and the wall following were employed for collision avoidance using the obstacle sparseness and the wall model, respectively. Here, the wall model could be obtained by the modified Hough transform overcoming the sonar sensor limitations. Next, the velocities of the robot were controlled for turnover avoidance in advance using the predicted terrain data. Here, to predict the front terrain data, the low-cost terrain sensor module was developed. Also, the operator could recognize the actual movement of the robot modified for collision and turnover avoidance by

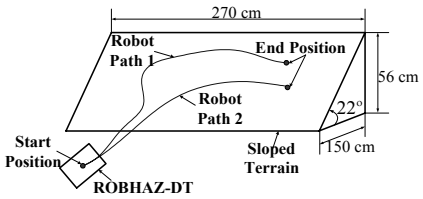

Fig. 12. Experimental Result of Turnover Avoidance

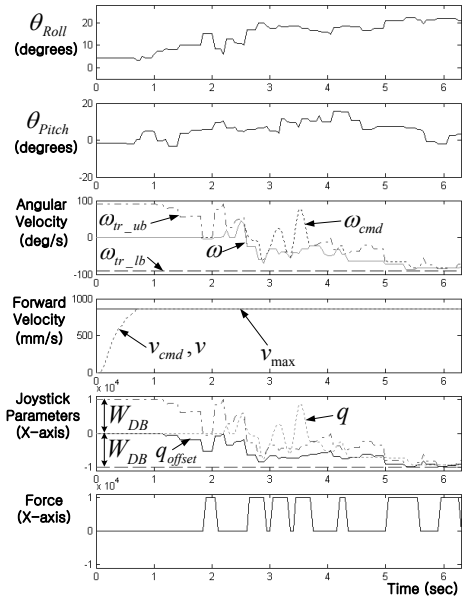

Fig. 13. Parameters about Experimental Result of Turnover Avoidance

force reflection. In experimental results for verifying the feasibility of the suggested methods, it was shown that the robot could move without collision and turnover in unknown environment.

ACKNOWLEDGEMENTS

This work was supported in part by the KIST.

REFERENCES

Bauzil, G., M. Briot and P. Ribes (1981). A navigation sub system using ultrasonic sensors for the mobile robot Hilare. *1st Int. Conf. on Robot Vision and Sensory Controls*, Stratford-upon-Avon, UK.

Borenstein, J. and Y. Koren (1989). Real-Time Obstacle Avoidance for Fast Mobile Robots. *IEEE Trans. on Systmes, Man, and Cybernetics,* **Vol. 19, No. 5**, pp.1179-1187.

Borenstein, J. and Y. Koren (1995). Error Eliminating Rapid Ultrasonic Firing for Mobile Robot Obstacle Avoidance. *IEEE Trans. on Robotics and Automation,* **Vol. 11, No. 1**, pp. 132-138.

Fukuda, T. and N. Kubota (1995). An Intelligent Robotic System Based on a Fuzzy Approach. *Proc. of the IEEE,* **Vol. 87, No. 9**, pp. 1448-1470.

Shiller, Z. and Y. R. Gwo (1991). Dynamic Motion Planning of Autonomous Vehicles. *IEEE Trans. on Robotics and Automation,* **Vol. 7, No. 2**, pp. 241-249.